PCCP

ROYAL SOCIETY OF CHEMISTRY

PAPER

View Article Online
View Journal | View Issue

Cite this: *Phys. Chem. Chem. Phys.*, 2025, **27**, 19852

Atmospheric reactions of substituted butanes with OH radicals: kinetics and atmospheric implications

Bishnupriya Kar[a] and Balla Rajakumar*[ab]

Received 11th March 2025,
Accepted 18th August 2025

DOI: 10.1039/d5cp00961h

rsc.li/pccp

2-Chlorobutane (2CB) and 2-aminobutane (2AB) are chiral compounds, which play a crucial role in biological complexity. These compounds can be released into the air through natural and man-made processes. Their emission into the atmosphere may influence the air quality and climate significantly. In the present work, the kinetics for the reactions of 2AB and 2CB were investigated experimentally and computationally at various temperatures. The rate coefficients for both reactions were evaluated using the SAR approach at 298 K. In addition, their impacts on the atmosphere have been discussed using atmospheric parameters. The experiments were performed using a pulsed laser photolysis – laser induced fluorescence technique for both reactions over 268–363 K. The rate coefficients were measured to be $(2.42 \pm 0.08) \times 10^{-12}$ and $(3.03 \pm 0.05) \times 10^{-11}$ cm^3 molecule^{-1} s^{-1}, for OH-initiated reactions of 2CB and 2AB, respectively. The computational calculations for these reactions were performed at the CCSD(T)/aug-cc-pVDZ//M06-2X/6-311+G(d,p) level of theory for 2CB and 2AB over 200–400 K. The rate coefficients were compared with changing the substituent on the butane chain. Cumulative atmospheric lifetime, radiative forcing, global warming potential, and acidification potential were calculated using the experimental and theoretical rate coefficients. In addition, the secondary organic compounds formed due to the reactions were analysed qualitatively using GC-MS and then compared with the theoretical results of the individual group contribution to the overall rate coefficients.

Introduction

2-Aminobutane (*sec*-butylamine, 2AB) and 2-chlorobutane (*sec*-butyl chloride, 2CB) are structurally important α-chiral compounds. Chiral compounds are important for biological systems, and primary amines and alkyl halides, in particular, are widely used in pharmaceutical and food industries.[1–3]

2AB is a fumigant fungicide with a high potential for bioaccumulation. Although it is not authorized for fungicidal applications within the European Union, it continues to serve as an antifungal agent in agricultural practices.[4] 2AB is used as a food preservative and fungistatic.[5] It is found in many vegetables.[6] It is a bioactive compound with fungicidal and pesticidal properties.[7,8] It is effective against Penicillium infection.[9] (*S*)-2AB is a precursor in the synthesis of tumor necrosis factor-α inhibitors[10] and is used in the synthesis of flavouring agents.[11] 2AB is found to be present in CO_2 capture units[12] and has been identified in tobacco smoke.[13] Short-chain chlorinated paraffins are utilized in various applications, including lubricant additives, metalworking, leather fat-liquoring, plastic softening, PVC plasticizers, and as flame retardants in paints, adhesives, and sealants, due to their high viscosity and excellent flame resistance. 2CB is one of such monochlorinated paraffins.[14] It is also used as a solvent in industries and laboratories.[15–17] It is used in the preparation of surfactant, resin, rubber, plasticizer, and pharmaceutical ingredients.[18] In addition, 2CB is used in *sec*-butyllithium synthesis.[19]

The extensive use of these compounds leads to their emission into the atmosphere. 2AB has been identified in the atmosphere surrounding fruits. Fruits and potatoes are fumigated using 2AB, which vaporizes readily and spreads evenly throughout the air in the storage room.[20,21] Aliphatic amines are mainly found in rainwater, at a concentration of <0.002–2.7 μmol N dm^{-3}.[22] No data are currently available to estimate the global or regional atmospheric deposition rates of amines.[23] Amines are present in the air at parts per billion (ppb) levels near agricultural operations, according to recent studies.[24] Rabaud *et al.*[25] measured various amines at a dairy, with butylamine concentrations reaching up to 560 μg m^{-3} (187 ppb). Murphy *et al.*[26] performed chamber experiments to study particulates formed from amines. Their research revealed that primary and secondary amines form salts, while tertiary amines react with OH radicals and ozone to produce non-salt secondary organic aerosols. Additionally, various chlorinated volatile organic compounds (VOCs) are present in the atmosphere,

[a] *Department of Chemistry, Indian Institute of Technology Madras, Chennai, 600036, India. E-mail: rajakumar@zmail.iitm.ac.in*
[b] *Centre for Atmospheric and Climate Sciences, Indian Institute of Technology Madras, Chennai, 600036, India*

with concentrations typically ranging from less than 1 μg m^{-3} to 10 μg m^{-3}.[27] Some C1–C3 chlorinated compounds are emitted into the atmosphere in Tg $year^{-1}$, and some are in Gg $year^{-1}$. No data is reported on the concentration of C4-chlorinated VOCs in the atmosphere.[28] The emitted compounds can be removed by several atmospheric processes such as atmospheric oxidation, photolysis, and wet and dry deposition of particles.

A study of the kinetics of these reactions in the atmosphere is necessary, especially with OH radicals and Cl atoms. OH radicals are highly abundant in the atmosphere, whereas the Cl atom-initiated reaction rates are comparatively higher than those of OH atom-initiated reactions, which has been observed in several reactions. This trend has been observed in the kinetics of various VOCs. For example, the reaction of *n*-butanol with Cl atoms proceeds approximately 25 times faster than with OH radicals.[29] Similarly, methyl propyl ether exhibits a ~23 fold higher reactivity with Cl atoms than with OH radicals.[30] The Cl-initiated reaction of 2,3-dichloropropene is about 9 times faster than its OH reaction.[31] For 2,3,3,3-tetrafluoropropene, the Cl-initiated reaction occurs ~67 times faster than the OH-initiated one.[32]

Other chlorobutane isomers also show a similar pattern: 1-chlorobutane reacts ~52 times faster with Cl atoms than with OH radicals, while iso-butyl chloride and *tert*-butyl chloride show increases of ~37 and ~32 times, respectively.[33–36] In our study, 2-chlorobutane (2CB) also demonstrated significantly higher reactivity, about 24 times, with Cl atoms compared to OH radicals.[33,34]

Despite the faster kinetics of Cl-initiated reactions, OH-initiated reactions typically dominate atmospheric degradation processes due to the much higher atmospheric abundance (10^6 radicals cm^{-3}) of OH radicals under ambient conditions.

The temperature-dependent kinetics for the reaction of 2CB with Cl atoms have been reported previously.[33] Loison *et al.*[34] investigated the kinetics for the reaction of 2CB with OH radicals at 298 K using laser-induced fluorescence (LIF). Currently, no temperature-dependent studies exist on the reaction of 2CB with OH radicals, and the reaction kinetics of 2AB with OH radicals have not been reported.

This study investigated the temperature-dependent kinetics of the reactions between 2CB and 2AB with OH radicals using both experimental and computational approaches.

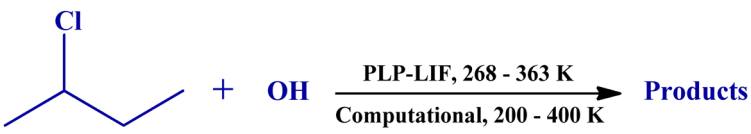

(R1)

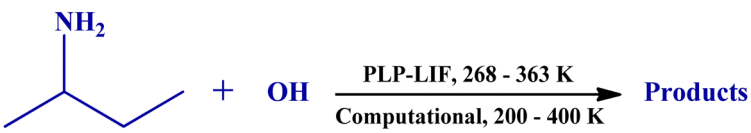

(R2)

The pulsed laser photolysis – laser induced fluorescence (PLP–LIF) method was used for the experiment. Computational techniques were employed to enhance the understanding of these compounds' degradation processes. The kinetics and branching ratios over an atmospheric temperature range of interest were also calculated. The atmospheric lifetime of the compounds, due to the reactions with OH radicals, was calculated by incorporating the rate coefficients obtained from the experiments. Atmospheric parameters such as global warming potential and acidification potentials of the studied compounds are also presented. The main products generated during the reactions were analysed using gas chromatography-mass spectrometry (GC-MS), and the reaction mechanism was proposed based on the identified products.

Experimental method

PLP–LIF technique

The experiments of the title reactions were carried out in a flow tube reactor. The reactor is a double-jacketed Pyrex cell typically designed for temperature-dependent kinetics studies. A thermal fluid was circulated through the outer layer of the jacket to maintain the temperature of the reaction cell using a thermal controller. The experiments were performed over a temperature range of 268–363 K. The temperature was measured using a K-type thermocouple. A detailed reaction setup is described elsewhere.[37] A brief discussion of the method is mentioned here. The reactions were initiated by photolyzing H_2O_2 at 248 nm with a KrF excimer laser (5 Hz, laser energy = 10–20 mJ cm^{-2}). The 2nd harmonic output of the Nd:YAG laser was used to pump a wavelength-tunable dye laser. Rhodamine-6G dye was used to produce a radiation with a wavelength of 563.8 nm, which was frequency doubled (281.9 nm) to probe the OH radicals generated from the H_2O_2. Both laser beams meet each other at the center of the cell, which is defined as the reaction zone. The emitted OH fluorescence (309 nm) passes through a bandpass filter (310 nm, fwhm = 10 nm) and is collected by a photomultiplier tube. The laser beams (both photolysis and probe) and photomultiplier tube were at a right angle to each other to avoid unwanted radiations such as scattering.

The reaction compound, precursor, and nitrogen gas flowed through the cell continuously, with the gas flow rates regulated by calibrated mass flow controllers (calibration curves are shown in the SI). The flows of H_2O_2 and N_2 gas were kept constant during the experiment at each temperature. The

sample flow was increased to perform the experiments at different concentrations, ultimately changing the total pressure (19–31 Torr) of the reaction cell. The reactions were carried out at pseudo-first-order conditions. The concentrations of the compounds and H_2O_2 were maintained in the order of $\sim 10^{14}$ molecule cm^{-3}. The concentration of OH radicals was measured using the concentration of H_2O_2, laser fluence (F), quantum yield (φ = 2), and absorption cross-section $\left(\sigma_{H_2O_2}^{248nm} = \sim 8.3 \times 10^{-20}\ cm^2\ molecule^{-1}\right)$[38] of OH radicals.

$$[OH] = [H_2O_2] \times F \times \varphi \times \sigma_{H_2O_2}^{248nm} \quad (E1)$$

The decay in the OH radical concentration ($[OH]_0 \approx 10^{11}$ radical cm^{-3}) with reaction time (t) was measured during the experiment. The reaction time is the delay of the probe laser beam after the photolysis laser beam. A graph is plotted using the equation as follows and the pseudo-first-order rate coefficients (k') were obtained.

$$\mathrm{Ln}\frac{I_t}{I_0} = -k't \quad (E2)$$

The bimolecular reaction rate coefficients (k_{A+OH}) were obtained from the plots of the pseudo-first-order rate coefficient *versus* the concentration of compound A at a given temperature, using the following equation.

$$k' = k_0 + k_{A+OH}[A] \quad (E3)$$

where k_0 is the rate coefficient in the absence of the compounds and the loss of OH radicals occurs due to their reaction with H_2O_2 and the diffusion of OH radicals out of the reaction zone.

Product analysis

Experiments were conducted to investigate the products formed from the reactions at room temperature and pressure using a Pyrex cell with a volume of 2405 cm^3. The reactions were carried out in the presence of O_2, with the cell being filled with a mixture of the sample (2CB or 2AB), H_2O_2, and O_2. N_2 served as the bath gas throughout the experiment. The gas mixture was left undisturbed for 1 hour to ensure homogenization. After photolysis, the gas mixture was injected into a GC-MS (7890B GC and 5977A MSD, Agilent Technologies). A DB-VRX capillary column was employed in the GC-MS analysis, with He as a carrier gas. During the analysis, the temperature was initially set at 35 °C for 15 minutes, then raised to 100 °C at a rate of 5 °C per minute. The temperature of 100 °C was held for 5 minutes. The source temperature was maintained at 150 °C, and the MS quadrupole was adjusted to 200 °C.

Materials

The experiments utilized 2CB (99%, Sigma Aldrich) and 2AB (≥99%, Sigma Aldrich), both of which were subjected to multiple freeze–pump–thaw cycles prior to use. Gaseous compound, helium (He: 99.999%) from Praxair India Pvt. Ltd, as well as nitrogen (N_2: 99.9992%) and oxygen (O_2: 99.85%) from Indogas Pvt. Ltd, were used as supplied. Additionally, a 30% H_2O_2 solution (ThermoFisher Scientific, Qualigens) was concentrated to approximately 85% (determined by titration with a standard solution of $KMnO_4$) by continuous nitrogen purging over several days before use.

Computational method

Computational calculations were carried out to study the kinetics of the title reactions. The kinetic calculations were performed at a dual level of theory, utilizing optimised structures (reactant (R), product (P), transition state (TS), and reactant complex (RC)) that were obtained using the M06-2X/6-311+G(d,p)[39–41] method in Gaussian16.[42] The geometries were visualized using GaussView 6.0 software.[43] The frequency calculations were carried out along with optimisation of the stationary points involved with the reactions. The M06-2X method is widely used for its reliability for the optimisation and frequency calculations balancing performance and computational cost. It is also observed that it is reliable for the thermochemistry and kinetics calculations for various reactions including unsaturated ketones, cycloalkene, alkenes, bicyclic compounds, such as 5-hexen-2-one/4-hexen-3-one + OH,[44] 1,4-cyclohexadiene + OH,[45] and 1,4-pentadiene + OH,[46] aniline + OH,[47] and adenine + OH.[48]

The reaction paths were drawn from the transition state to reactants and products using the intrinsic reaction coordinate (IRC) method. The rate coefficients were calculated using the polyrate-17C/Gaussrate-17B[49,50] program suite. The conformers of stationary points were found using MSTor, and the most stable conformer was used in the calculation.

The CVT/SCT rate coefficients ($k^{CVT/SCT}(T)$) were calculated using the following equations.

$$k^{CVT/SCT}(T) = \kappa^{SCT}(T)k^{CVT}(T) \quad (E4)$$

where,

$$k^{CVT}(T) = \min_s k^{GT}(T,s) = k^{GT}[T,s^{CVT}(T)] \quad (E5)$$

and

$$k^{GT}(T,s) = \sigma \frac{k_B T}{h}\left(\frac{Q^{GT}(T,s)}{Q^{R}(T)}\right)\exp\left(\frac{-V_{min}(s)}{k_B T}\right) \quad (E6)$$

Here $k^{CVT}(T)$ represents the CVT rate coefficient, and $\kappa^{SCT}(T)$ is the transmission coefficient at temperature T. The symbol s indicates the position of the generalised TS along the minimum-energy reaction path, while σ refers to the symmetry factor, and k_B and h retain their usual meanings. Q^{GT} and Q^{R} are the partition functions for the generalised TSs and the reactants, respectively. V_{min} denotes the potential of the generalised TS along the minimum-energy reaction path.

Single point energies used in the calculation of CVT/SCT/ISPE rate coefficients were obtained at the CCSD(T) level of theory using the aug-cc-pVDZ basis set for 2CB and 2AB. The T1 diagnostic values of stationary points in the key reaction pathways, as obtained from CCSD(T) calculations, were examined to assess multireference characteristics.

The frequencies were scaled for the kinetic calculations, and the scale factor used was 0.970. Non-redundant curvilinear

internal coordinates for generalized normal mode analysis along the minimum energy reaction path were employed in the calculation of rate coefficients. The individual rate coefficients for each reaction were summed for the overall rate coefficients for the title reactions.

The multi-structural method with torsional anharmonicity (MS-T)[57–59] separates translational and electronic partition functions from the conformational–rotational–vibrational part. It takes into account multiple torsional degrees of freedom in polyatomic molecules, resulting in various conformations for reactants and TSs. This leads to a change in the partition functions and influences the calculated rate coefficients. The multi-structural torsional anharmonicity factor (F) was employed to measure the effect of torsional anharmonicity on the reaction rate. The partition functions were computed from geometries, energies, and Hessians derived using the M06-2X/6-311+G(d,p) method.

The C1 symmetry of the reactants and TSs indicates that the external symmetry number is 1 and each species has two optical isomers, which is taken into account in the calculations. The electronic partition function of the reactants (2CB and 2AB) and TSs were set to the spin multiplicity and is equal to 1 for reactant and 2 for TSs. The temperature-dependent electronic partition function of OH radical was calculated by including the splitting of the ground-state into the $^2\Pi_{3/2}$ and $^2\Pi_{1/2}$ states (ΔE_{SO} = 139.7 cm^{-1}),[60] due to spin–orbit interaction, and have quantum weights of 2 and 2, respectively.

The kinetic branching ratio (Γ), which defines the proportion of the rate coefficient of a specific site (k_i) relative to the overall rate coefficient (k), was calculated for all reaction sites using the equation as follows.

$$\Gamma\ (\%) = \left(\frac{k_i}{k}\right) \times 100 \qquad \text{(E7)}$$

Structure–activity relationship (SAR)

The SAR in the gas-phase kinetics of VOCs with OH radicals involves understanding how the molecular structure of VOCs influences their reaction rates and mechanisms when interacting with OH radicals. In this work, the SAR was used to evaluate the kinetics for the reactions of 2CB and 2AB with OH radicals.

The rate constants for the H abstraction by OH radicals proposed by Kwok and Atkinson[61,62] were used in the calculation of rate coefficients of the title reactions at 298 K. The rate constants are as follows:

The data for the kinetics of the reactions can be represented using the following equations, where k_{prim}, k_{sec}, and k_{tert} are the rate constants for reactions involving the –CH_3, –CH_2–, and –CH$\leq$ groups, respectively when X, Y, and Z are each methyl groups:

$$k(\text{X–CH}_3) = k_{prim}F(\text{X}) \qquad \text{(E8)}$$

$$k(\text{X–CH}_2\text{–Y}) = k_{sec}F(\text{X})F(\text{Y}) \qquad \text{(E9)}$$

$$k(\text{X–CH}\leq^{\text{Y}}_{\text{Z}}) = k_{tert}F(\text{X})F(\text{Y})F(\text{Z}) \qquad \text{(E10)}$$

where F(X), F(Y), and F(Z) represent the factors for the substituents X, Y, and Z, respectively.

The H abstraction rate constants (in 10^{-12} cm^3 molecule^{-1} s^{-1}) for the –CH_3, –CH_2–, –CH$\leq$, and –NH_2 groups are k_{prim} = 0.130, k_{sec} = 0.769, k_{tert} = 1.49,[63] and k_{NH_2} = 19.[64] The factors are F(–CH_3) = 1.00, F(–CH_2–) = F(–CH$\leq$) = 1.35,[63] F(–Cl) = 0.38,[62] and F(–NH_2) = 7.4.[64]

Results and discussion

Experimental section

The temperature-dependent rate coefficients were measured over a range of 268–363 K for both reactions (R1) and (R2) using the PLP–LIF method. Experimental conditions and the rate coefficients for both reactions at 298 K are listed in Tables 1 and 2. The data measured for the kinetics of both reactions at all temperatures are provided in Tables S1 and S2 in the SI.

Reaction 2CB + OH. Fig. 1a displays a pseudo-first-order plot for reaction (R1) at 298 K. The decay of LIF intensity due to the presence of the gaseous sample (2CB) with the reaction time (delay time) was observed. The decay is faster with increasing concentrations of the gaseous sample, as shown in Fig. 1a, according to eqn (E3). The reaction rate coefficient was determined based on the pseudo-first-order rate coefficients and the concentrations of the gaseous sample. At 298 K, the bimolecular rate coefficient for reaction (R1) was determined to be $(2.42 \pm 0.08) \times 10^{-12}$ cm^3 molecule^{-1} s^{-1}, based on the slope of the plot in Fig. 1b. The temperature-dependent rate coefficients for reaction (R1) at all temperatures are summarized in Table 1. The rate coefficients were found to be decreasing with the increasing temperature from 268 K to 363 K, as shown in Fig. 1b. It can be described by the Arrhenius expression.

$$k_{2CB}^{PLP-LIF}(T = 268\text{–}363\ \text{K}) = (5.27 \pm 1.23) \times 10^{-13} \exp\{-(-463 \pm 143)/T\}\ \text{cm}^2\ \text{molecule}^{-1}\ \text{s}^{-1}$$

The quoted errors given in the expression are in 2σ of the least square fitting. The activation energy was found to be (-0.92 ± 0.28) kcal mol^{-1} from the Arrhenius equation.

The pressure was varied (though it is a very small range: 21–54 Torr) by varying the flow rate in the reaction cell using mass flow controllers, which in turn has changed the precursor concentration. However, this short range is not suitable to comment on the pressure dependence of the rate coefficients. The kinetic measurements for the reaction of 2CB with OH radicals at 298 K were performed by varying the laser fluence as

Table 1 PLP–LIF experimental kinetics data for the reaction 2CB + OH across the temperature range of 268–363 K

Temperature (K)	Total pressure (Torr)	$[2CB]/10^{15}$ (molecule cm^{-3})	$k_{2CB+OH}^{PLP-LIF}/10^{-12}$ (cm^3 molecule^{-1} s^{-1})
268	21–22	0.23–1.01	3.09 ± 0.26
283	19–20	0.19–1.16	2.52 ± 0.34
298	21–22	0.21–1.34	2.42 ± 0.16
318	19–22	0.19–1.34	2.39 ± 0.20
343	19–22	0.19–1.34	2.11 ± 0.22
363	25–26	0.23–1.75	1.81 ± 0.16

Table 2 PLP–LIF experimental kinetics data for the reaction 2AB + OH over 268–363 K

Temperature (K)	Pressure (Torr)	$[2AB]/10^{14}$ (molecule cm^{-3})	$k_{2AB+OH}^{PLP-LIF}/10^{-11}$ (cm^3 molecule^{-1} s^{-1})
268	30–31	0.33–2.00	3.71 ± 0.16
283	30–31	0.33–1.93	3.46 ± 0.20
298	26–27	0.29–1.74	3.03 ± 0.10
318	27–28	0.30–1.74	2.60 ± 0.16
338	27–28	0.30–1.80	2.25 ± 0.14
363	30–31	0.34–1.93	1.68 ± 0.12

well. The rate coefficients remained unchanged within the error range (see Table S3 in the SI).

Reaction 2AB + OH. A PLP–LIF experiment was performed to investigate the kinetics of the 2AB + OH reaction within the range 268–363 K. The pressure of the reaction cell and the concentrations of 2AB are listed in Table 2. The rate coefficients for reaction (R2) were obtained from the plot of pseudo-first-order rate coefficients against concentrations of 2AB, as shown in Fig. 2a. The pseudo-first-order rate coefficients were calculated from the plot of LIF intensity against reaction time, as shown in Fig. 2a. At 298 K, the rate coefficient for reaction (R2), derived from the slope of the plot shown in Fig. 2b, was found to be $(3.03 \pm 0.05) \times 10^{-11}$ cm^3 molecule^{-1} s^{-1}. The kinetics investigated at various temperatures over 268–363 K, as shown in Fig. 2b, are described by the Arrhenius equation.

$$k_{2AB}^{PLP-LIF}(T = 268\text{–}363\ K) = (2.04 \pm 1.05) \times 10^{-12} \exp\{-(-795 \pm 158)/T\}\ cm^3\ molecule^{-1}\ s^{-1}$$

A negative temperature dependence was observed throughout the investigated range. The activation energy from the experimental Arrhenius equation was found to be (-1.58 ± 0.31) kcal mol^{-1}. The errors in the expression represent the 2σ

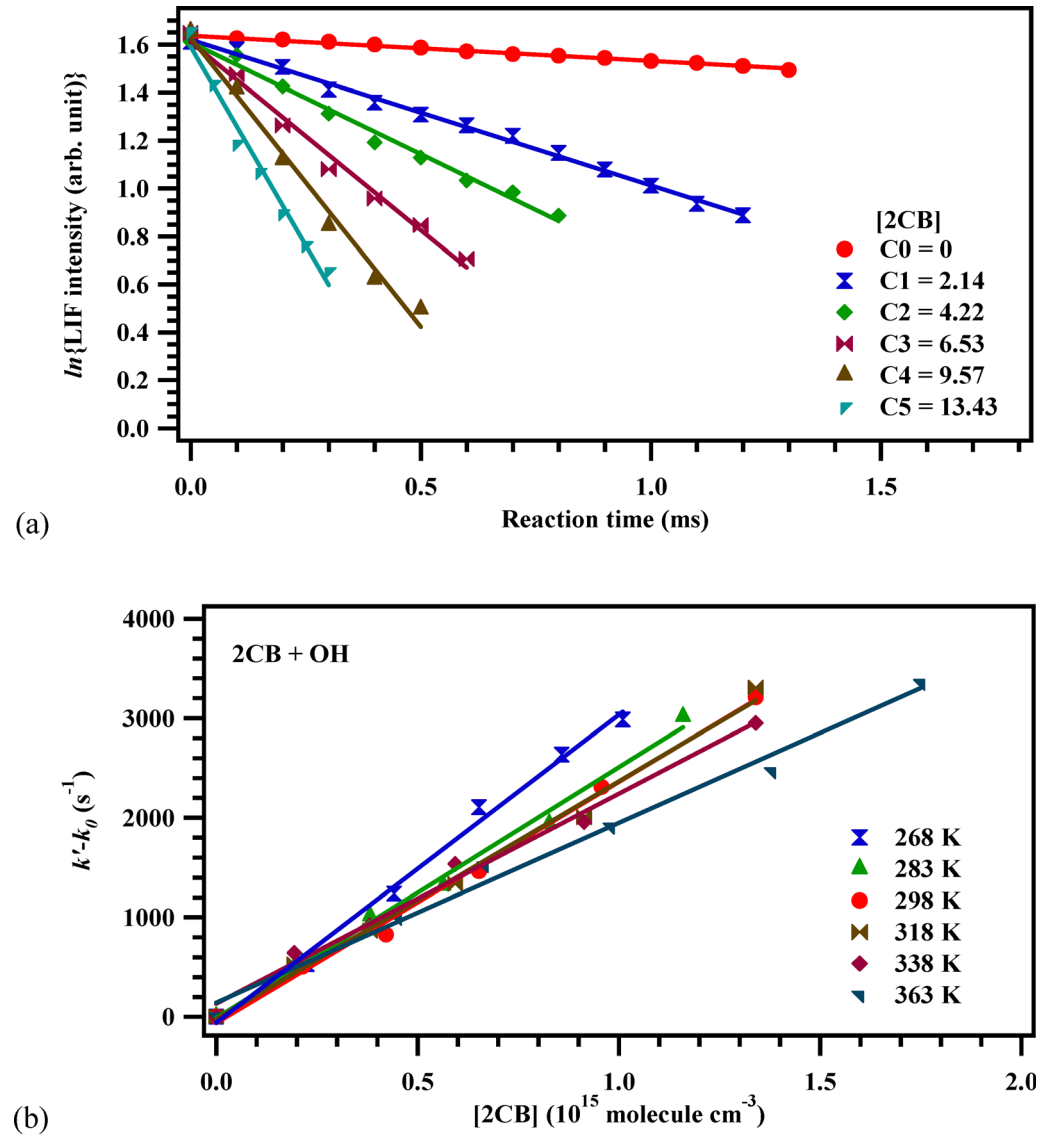

Fig. 1 (a) Variation of LIF intensities with reaction time at 298 K; C0, C1, C2, C3, C4, and C5 are the concentrations (10^{15} molecule cm^{-3}) of 2CB and (b) $(k' - k_0)$ with the concentration of 2CB at different temperatures for the reaction of 2CB with OH radicals over the range of 268–363 K.

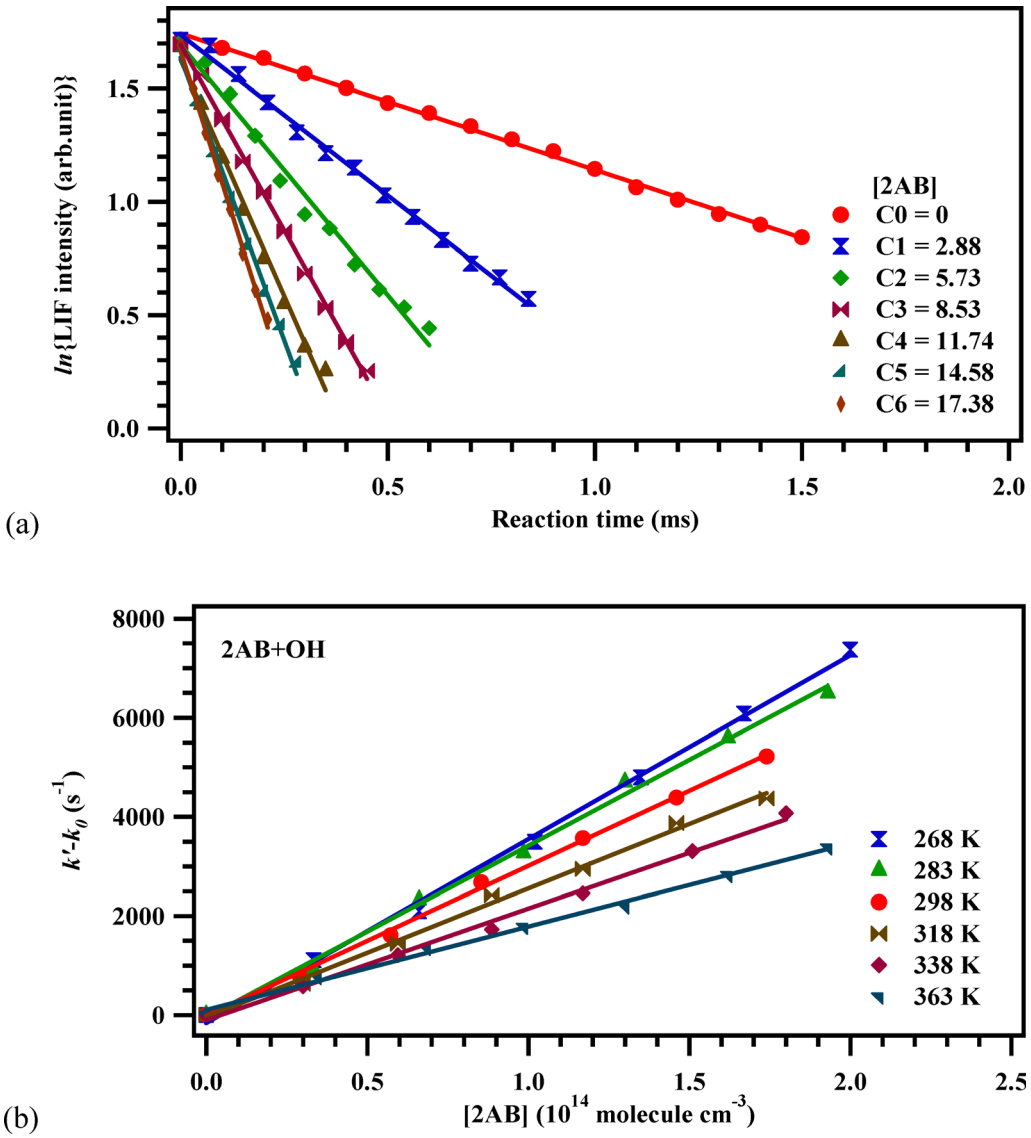

Fig. 2 (a) Variation of LIF intensities with reaction time at 298 K; C0, C1, C2, C3, C4, and C5 are the concentrations (10^{14} molecule cm^{-3}) of 2AB and (b) ($k' - k_0$) with the concentration of 2AB at different temperatures for the reaction of 2AB with OH radicals over 268–363 K.

of the least square fitting. The kinetics were found to be insensitive (see Table S4 in the SI), varying the laser fluence.

Computational calculations

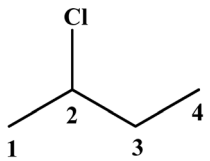

2-chlorobutane (2CB)

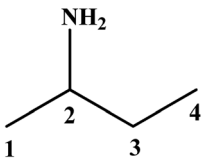

2-aminobutane (2AB)

The geometries involved in the reactions of 2CB and 2AB with OH radicals are analysed using the MSTor software, and the most stable geometries were used in the calculation. The optimised most stable geometries at the M06-2X/6-311+G(d,p) level of theory are shown in Fig. S1 and S2. Tables S5–S8 provide the Cartesian coordinates for the geometries and the vibrational frequencies. The TSs were identified with a single imaginary frequency of ($3n - 6$) frequencies. Here, n denotes the number of atoms in the molecule. In addition, the TSs were verified with IRC, which connect TSs to the reactants and products along minimum energy reaction path. These are shown in Fig. S3 and S4.

Thermochemistry. Thermochemical analysis for both reactions was conducted using the M06-2X/6-311+G(d,p) level of theory. The reaction enthalpy and free energy of the reaction at 298 K are presented in Tables S9 and S10. OH radicals can abstract H atoms directly from carbon or nitrogen atoms. There are four products in the OH reaction of 2CB. P3 ($\Delta H^\circ = -15.83$ kcal mol^{-1}, $\Delta G^\circ = -17.83$ kcal mol^{-1}) was found to be the most feasible and the most stable product following the product P2 ($\Delta H^\circ = -15.73$ kcal mol^{-1}, $\Delta G^\circ = -17.49$ kcal mol^{-1}).

The other two products P1 and P4 are less stable and feasible than P2 and P3, *i.e.*, the secondary H abstractions are more feasible and form more stable products than the primary H abstraction. In the case of the reaction of 2AB, there are five reaction sites for H abstraction, which form five products: P1, P2, P3, P4, and P_N. Among these, P1, P2, P3, and P4 are formed by the H abstraction from C atoms, whereas P_N is formed as a result of H abstraction from the N atom. The product P2 (ΔH° = −26.16 kcal mol^{-1}, ΔG° = −27.81 kcal mol^{-1}) is the most stable and feasible thermodynamically among them all. The relative enthalpy of the other products P1, P3a, P3b, P4, and P_N lies between −15.9 and −18.64 kcal mol^{-1}, and the relative free energy lies between −17.69 and −20.91 kcal mol^{-1}.

Potential energy surface (PES). The diagram illustrating the PES corrected with zero-point energy (ZPE) for both reactions is provided in Fig. 3. The CCSD(T)/aug-cc-pVDZ//M06-2X/6-311+G(d,p) level of theory was used for the single point energy calculation of the stationary points. The single point energies were also calculated at the complete basis set (CBS) limit (an extrapolation from the aug-cc-pVDZ and aug-cc-pVTZ basis sets). The barrier energies were found to be higher at the CBS limit than that at the double-zeta level (see Tables S11 and S12).

The low T_1 diagnostic values ($\leq$0.03) as shown in Table S13 suggest that single-reference methods are sufficient for the calculation.[51,52] Thus, it is expected to provide reliable energetics for the reactions of 2CB and 2AB with OH radicals. The CCSD(T) approach is consistent with previous studies involving similar systems, such as the reactions of 1-chlorobutane,[53] methylamine,[54] methanolamine,[55] and tetrahydrofuran[56] with OH radicals, where CCSD(T) yielded accurate energetic data.

There are five unique reaction sites for H abstraction in 2CB, as shown in Fig. 3. The energy barrier for the reaction through TS2 (−1.34 kcal mol^{-1}) is the lowest, followed by TS3b and TS3a (−0.77 kcal mol^{-1} and −0.23 kcal mol^{-1}). The H abstraction through TS1 (1.60 kcal mol^{-1}) has the highest barrier, followed by TS4 (1.15 kcal mol^{-1}). Thus, it follows the trend: TS2 < TS3b < TS3a < TS4 < TS1. It is observed here that the H abstraction from the primary C atom needs more energy than the secondary C atoms. The H atom bonded to the carbon attached directly to the chlorine can proceed with the least energy than from another secondary C atom, as observed in the reaction of 2CB with Cl atoms.[33] The major reaction pathways *via* TS2, TS3a, and TS3b follow barrierless pathways, and the other two, TS1 and TS4, have slightly positive barriers relative to reactants. There exist pre-reactive complexes (RC2, RC3a, RC3b, and RC4) before corresponding TSs. P3 (−18.57 kcal mol^{-1}), formed through TS3, was found to be the most stable product formed in the title reaction, followed by P2 (−18.28 kcal mol^{-1}) formed through TS2. P4 (−14.50 kcal mol^{-1}), formed through TS4, is the least stable product next to P1 (−15.06 kcal mol^{-1}), formed through TS1.

The diagram depicting the PESs in reactions involving OH with 2AB is shown in Fig. 3. There are seven individual pathways for the H abstractions. The activation energies (relative energies are in units of kcal mol^{-1}) for the H abstraction from C1 (TS1), C2 (TS2), C3 (TS3a and TS3b), C4 (TS4), and N (TS_N1 and TS_N2) atoms in the reaction are −0.48, −2.27, −2.39, −2.72, −1.59, −1.39, and −1.41, respectively. The reaction through TS3b has the lowest barrier, followed by TS3a. The H abstraction from the primary CH_3 groups (TS4) has a lower

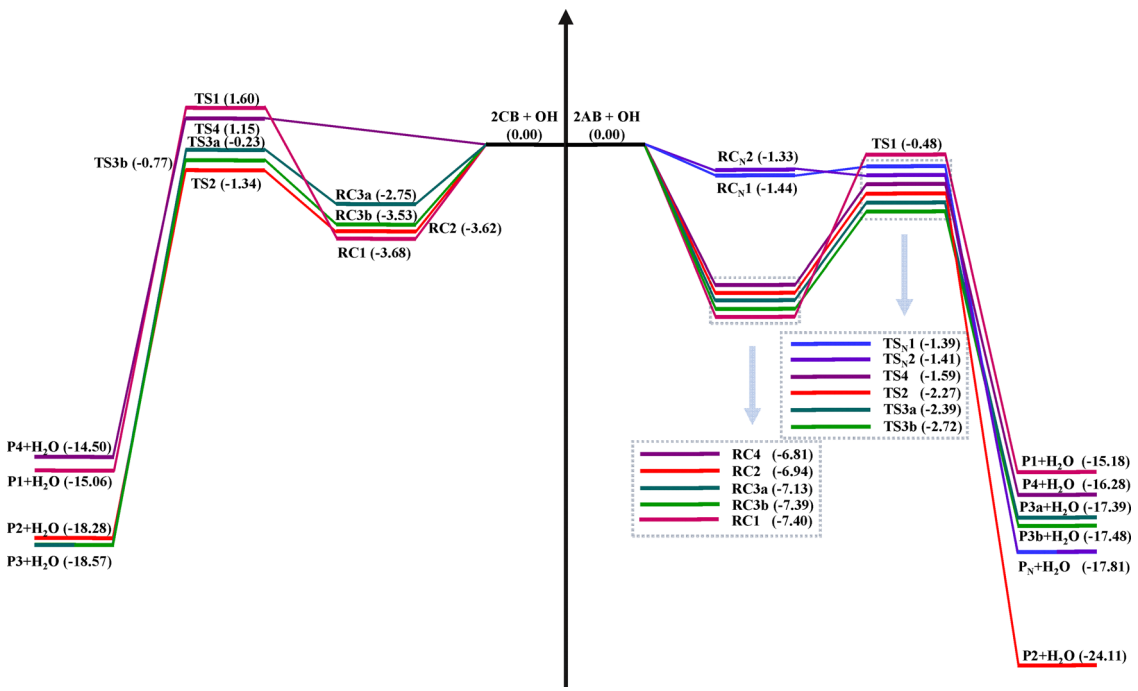

Fig. 3 Potential energy surfaces for the reactions of 2CB and 2AB with OH radicals, calculated at the CCSD(T)/aug-cc-pVDZ//M06-2X/6-311+G(d,p) level of theory with ZPE correction (*Y*-axis: not to scale).

barrier than that through TS_N1 and TS_N2, *i.e.*, from the $-NH_2$ group. It follows the trend TS3b < TS3a < TS2 < TS4 < TS_N2 < TS_N1 < TS1. The reaction pathways under investigation proceed through their respective RCs before reaching the TSs and forming the final products. Among these, the products resulting from TS_N1 and TS_N2 are energetically identical and are referred to as P_N, with a relative energy of −17.81 kcal mol^{-1}. The most stable product observed is P2, which has an energy of −24.11 kcal mol^{-1}. In contrast, the hydrogen abstraction processes from the C3 atom *via* transition states TS3a and TS3b yield products P3a and P3b, which are of similar energy, with relative energies of −17.39 kcal mol^{-1} and −17.48 kcal mol^{-1}, respectively. The H abstraction from the C4 atom results in P4, with an energy of −16.28 kcal mol^{-1}. The least stable product identified is P1, which has a relative energy of −15.18 kcal mol^{-1}.

The activation barriers of all TSs associated with 2AB for its reaction with OH radicals are lower than those of the similar TSs for the reaction of 2CB with OH radicals, suggesting that the reaction of 2AB with OH radicals proceeds at a faster rate compared to 2CB. Furthermore, the products resulting from H abstraction from the C2 atom of 2AB exhibit greater stability than those from 2CB. This increased stability can be attributed to the presence of the $-NH_2$ group. In contrast, the electron-withdrawing effect of the Cl atom in 2CB makes it less reactive than 2AB, where the $-NH_2$ group exerts a weaker electron-withdrawing influence. The presence of Cl decreases the electron density on the carbon chain, making it less reactive. Additionally, the electron-withdrawing nature of Cl in 2CB destabilises the product P2 more than in the case of 2AB, where the $-NH_2$ group stabilises the product P2.

Kinetics. The rate coefficients for both reactions were calculated using rectilinear and non-redundant curvilinear coordinates at a dual level of theory and are provided in Tables S14 and S15. The CVT/SCT/ISPE/MSTor method was applied for the calculations at the CCSD(T)/aug-cc-pVDZ//M06-2X/6-311+G(d,p) level of theory. Single point energies calculated at

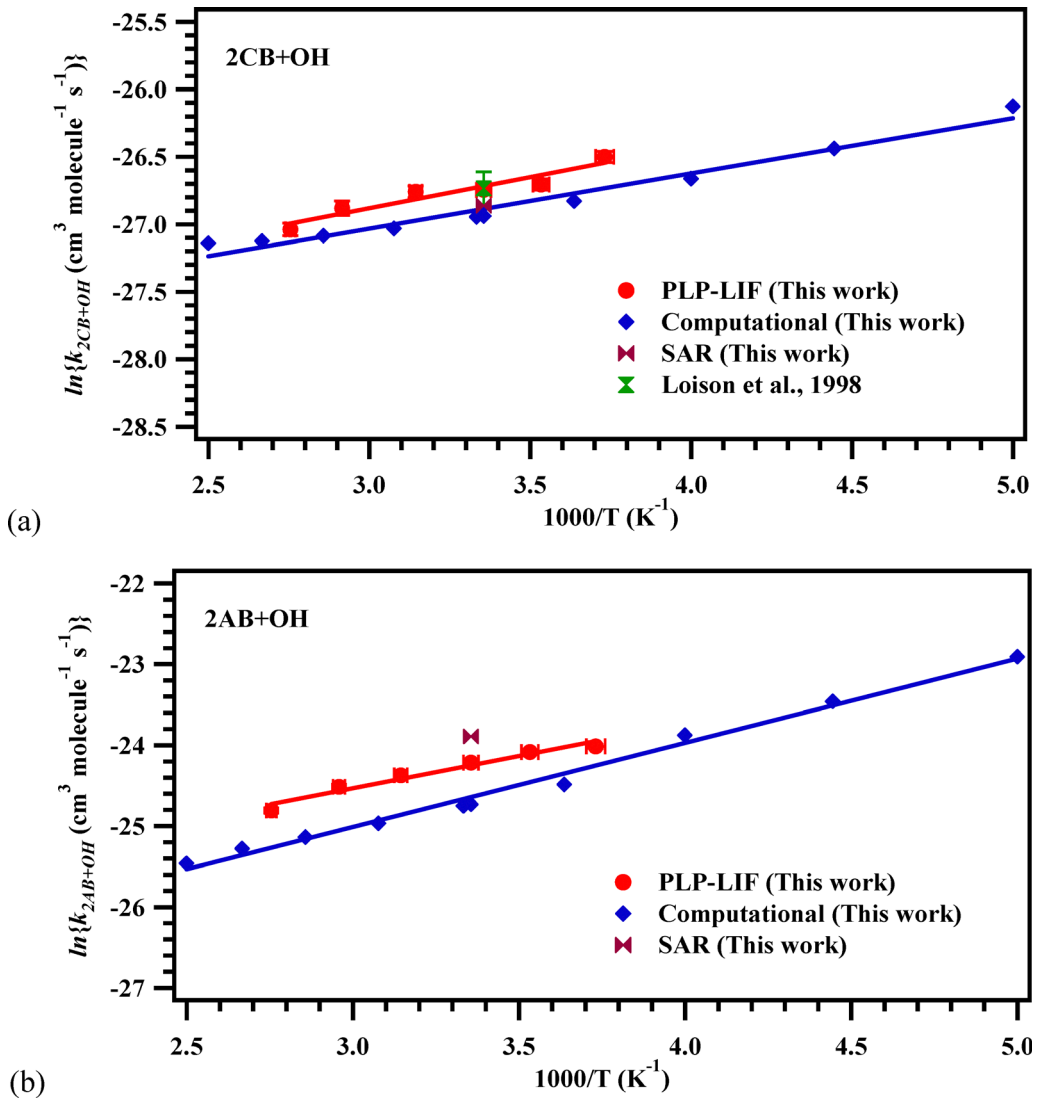

Fig. 4 Arrhenius plots for the reaction of (a) 2CB and (b) 2AB with OH radicals over the temperature range under study.

the CCSD(T)/aug-cc-pVDZ level were used to determine the CVT/SCT/ISPE rate coefficients. The rate coefficient calculations were also performed using the CBS limit. However, the rate coefficients obtained at the CCSD(T)/aug-cc-pVDZ//M06-2X/6-311+G(d,p) level were found to be in good agreement with the experimental results. The *F* factors (QMS-T/QSS-HO1) from the MSTor method (see Tables S16 and S17) were then employed to derive the final rate coefficients.

The rate coefficients for the OH-initiated reactions of 2CB and 2AB at 298 K were calculated to be 1.99×10^{-12} and 1.81×10^{-11} cm^3 molecule^{-1} s^{-1}, respectively. The rate coefficients exhibited a negative temperature dependence within the 200–400 K range. The corresponding Arrhenius equations are as follows.

$$k_{2CB}^{Theory}(T = 200\text{–}400\ K) = (5.31 \pm 0.97) \times 10^{-13} \exp\{-(-410 \pm 26)/T\}\ cm^3\ molecule^{-1}\ s^{-1}$$

$$k_{2AB}^{Theory}(T = 200\text{–}400\ K) = (6.04 \pm 1.56) \times 10^{-13} \exp\{-(-1040 \pm 36)/T\}\ cm^3\ molecule^{-1}\ s^{-1}$$

The rate coefficients calculated for both reactions across the examined temperature range are shown as a function of temperature in Fig. 4a and b. The negative temperature dependence and the negative Arrhenius activation energy may also be attributed to the stable RCs formed prior to TSs.

The rate coefficients for the reactions of 2CB and 2AB with OH radicals at 298 K were determined using the SAR approach. The SAR-derived rate coefficients are 2.15×10^{-12} cm^3 molecule^{-1} s^{-1} for 2CB and 4.20×10^{-11} cm^3 molecule^{-1} s^{-1} for 2AB. Computational calculations for these reactions show reasonable agreement with the values derived by the SAR approach.

Kinetic analysis. The values measured in this investigation and the computed rate coefficients for 2CB agree well. Additionally, our results at room temperature show good agreement with the rate coefficient $(2.45 \pm 0.30) \times 10^{-12}$ cm^3 molecule^{-1} s^{-1} reported by Loison *et al.*[34] The kinetics of the reaction between 2AB and OH radicals are being investigated for the first time in this study. It was observed that the presence of the –NH_2 group in 2AB enhances the rate coefficients, whereas the presence of a Cl atom in 2CB decreases the rate coefficients. As a result, this trend is followed by the rate coefficients for the reaction with OH radicals: 2CB ($(2.42 \pm 0.08) \times 10^{-12}$ cm^3 molecule^{-1} s^{-1}, this work) < butane ($(2.72 \pm 0.27) \times 10^{-12}$ cm^3 molecule^{-1} s^{-1})[65] < 2AB ($(3.03 \pm 0.05) \times 10^{-11}$ cm^3 molecule^{-1} s^{-1}, this work). It has been noted that the reaction of 2AB has the highest rate coefficient of all of them. This might be because the –NH_2 group has a weaker electron-withdrawing effect. On the other hand, the stronger electron-withdrawing action of the –Cl group makes 2CB less reactive.

Comparing the kinetics of OH-initiated reactions with chlorinated C4 compounds, a trend emerges where branching reduces the rate coefficients: 1-chlorobutane ($(2.22 \pm 0.50) \times 10^{-12}$ cm^3 molecule^{-1} s^{-1})[58] ≈ 2CB ($(2.42 \pm 0.08) \times 10^{-12}$ cm^3 molecule^{-1} s^{-1}, this work) > *tert*-butyl chloride ($(5.25 \pm 0.07) \times 10^{-13}$ cm^3 molecule^{-1} s^{-1}).[36] This trend is also observed for 2AB, where the rate coefficient for its reaction with OH radicals exceeds that of *tert*-butylamine ($(8.4 \pm 1.7) \times 10^{-12}$ cm^3 molecule^{-1} s^{-1}) at 298 K.[66] The reactivity in both 2CB and 2AB mainly depends on the feasibility of H abstraction and the stability of radical formation. Secondary H atoms are generally more reactive than primary ones due to the stability of secondary radicals. The greater the number of secondary H atoms, the greater the reactivity will be. In amino butanes, reactivity is enhanced by the number of secondary H abstractions, while the presence of the –NH_2 group can further affect the H abstraction process, influencing overall reactivity. It was observed that the reactivity decreases with the electron-withdrawing ability of substituents on the C2 atom. The electron-withdrawing effect of –NH_2, –OH, and –Cl is as follows: –NH_2 < –OH < –Cl. Thus, the rate coefficients at 298 K follow the trend: 2CB ($(2.42 \pm 0.08) \times 10^{-12}$ cm^3 molecule^{-1} s^{-1}, this work) < 2-butanol ($(8.77 \pm 1.46) \times 10^{-12}$ cm^3 molecule^{-1} s^{-1})[67] < 2AB ($(3.03 \pm 0.05) \times 10^{-11}$ cm^3 molecule^{-1} s^{-1}, this work).

The temperature dependencies of both reactions observed in the experiments show good agreement with the computational results. The rate coefficients at the temperatures at which the experiments were conducted, calculated using the Arrhenius equations described above, are presented in Table 3. When comparing the computational and experimental rate coefficients for the reaction of 2CB with OH over the temperature range, the computational values exhibit greater variation at lower temperatures. In contrast, for the reaction of 2AB with OH radicals, the computational rate coefficients show more pronounced changes at higher temperatures.

The negative temperature dependence of these reactions also shows good agreement with that of 2-butanol, as reported in previous studies by Jimenéz *et al.*, McGillen *et al.*, and Zheng *et al.*[67–69]

Reactivity trends. The positive temperature dependence of the rate coefficients for the reactions of monochlorinated alkanes with OH radicals decreases with the increase in the length of the C chain. Chloromethane shows the largest positive dependence on temperature, whereas this effect diminishes in the succeeding chloroalkanes.[70,71] Several studies have reported the temperature dependence of chloromethane and chloroethane.[70–73] However, similar reports for the larger chloroalkanes, starting from chloropropane, are sparse in the literature. Only two studies have reported the temperature dependent rate coefficients for chlorinated propane.[72,74] It is observed that the temperature dependency reported by Yujing and Mellouki[74] is much less positive

Table 3 Computationally obtained rate coefficients for the reactions of 2CB and 2AB with OH radicals at the CCSD(T)/aug-cc-pVDZ//M06-2X/6-311+G(d,p) level for the temperature range of 268–363 K

T (K)	$k_{2CB+OH}^{Theory}/10^{-12}$ (cm^3 molecule^{-1} s^{-1})	$k_{2AB+OH}^{Theory}/10^{-11}$ (cm^3 molecule^{-1} s^{-1})
268	2.45	2.93
283	2.26	2.38
298	1.99	1.81
318	1.93	1.59
343	1.75	1.25
363	1.64	1.06

Table 4 Comparison of activation energies of analogous compounds of 2-chlorobutane

Molecule	E_a (kcal mol^{-1})	Temperature range (K)	Method	Ref.
Chloromethane	2.66 ± 0.40	240–300	Review	Atkinson *et al.*, 2001[70]
	2.46	220–380	PLP–LIF	Herndon *et al.*, 2001[71]
Chloroethane	2.15 ± 0.72	296–360	PR–UV[a]	Markert and Nielsen, 1992[72]
	1.58 ± 0.07	294–448	PLP–LIF	Kasner *et al.*, 1990[73]
1-Chloropropane	2.89 ± 0.96	295–353	PR–UV[a]	Markert and Nielsen, 1992[72]
	1.04 ± 0.10	233–372	PLP–LIF	Yujing and Mellouki, 2001[74]
2-Chloropropane	2.63 ± 1.67	295–353	PR–UV[a]	Markert and Nielsen, 1992[72]
	0.72 ± 0.13	233–372	PLP–LIF	Yujing and Mellouki, 2001[74]
1-Chlorobutane	1.67 ± 0.96	295–353	PR–UV[a]	Markert and Nielsen, 1992[72]
2-Chlorobutane	−0.92 ± 0.28	268–363	PLP–LIF	This work
tert-Butyl chloride	0.28 ± 0.10	268–363	PLP–LIF	Joy and Rajakumar, 2023[36]
Isobutyl chloride	−0.08 ± 0.16	268–363	PLP–LIF	Joy and Rajakumar, 2025[35]
1-Chloropentane	0.96 ± 0.72	295–353	PR–UV[a]	Markert and Nielsen, 1992[72]
1-Chlorohexane	0.72 ± 0.48	295–353	PR–UV[a]	Markert and Nielsen, 1992[72]
Methyl amine	−0.45 ± 0.30	299–426	FP–RF[b]	Atkinson *et al.*, 1977[76]
Ethyl amine	−0.38 ± 0.31	298–426	FP–RF[b]	Atkinson *et al.*, 1978[77]

[a] PR–UV: pulse radiolysis–UV. [b] FP–RF: flash photolysis–resonance fluorescence.

than that reported by Markert and Nielson.[72] The temperature-dependent rate coefficients for the reactions of 1-chlorobutane, 1-chloropentane, and 1-chlorohexane were only reported by Markert and Nielsen.[72] The temperature-dependent rate coefficients reported by Joy and Rajakumar[35] for the reaction of *tert*-butyl chloride show a positive trend, whereas it is independent of temperature for the reaction of isobutyl chloride.[36] The rate coefficients reported by Markert and Nielsen[72] have significant scattering and error, which leads to less reliability on the temperature-dependence reported by them. The activation barriers for the overall reactions of monochlorinated alkanes are given in Table 4. The values suggest that the positive temperature dependence diminishes significantly from chloromethane to 1-chlorohexane. It should be noted that the shifting of the Cl-atom substitution from the terminal position also leads to a marked decrease in the overall positive temperature dependence. Hence, although it may seem that the rate coefficients of the monochlorinated alkanes may have a positive dependence on temperature at first glance, the decrease of this effect due to increasing size coupled with the effects of substituent positions indicates that this may not be a simple trend. Thus, although unexpected, it is not too surprising to see a negative temperature dependence in the case of 2-chlorobutane, as reported in this work.

A few temperature-dependent kinetic studies reported the rate coefficients for the OH radical reaction of primary amine, *i.e.*, for methyl amine (MA) and ethyl amine (EA). Onel *et al.*[75] and Atkinson *et al.*[76,77] reported a negative temperature dependency for the OH radical reactions of MA and EA. Onel *et al.* mentioned that both reactions are collisionally controlled, whereas the activation barriers reported by Atkinson *et al.* are shown in Table 4 for both reactions. Thus, the trend of temperature dependency cannot be concluded for the OH reactions of amine with an increase in chain length and the position of the substituent due to their limited studies.

Kinetic branching ratio (%). Fig. 5a and b show the branching ratios for individual channels as a function of temperature, which were computed for both processes. The calculated branching ratio (%) data are listed in Tables S18 and S19. The branching ratios are directly calculated by incorporating multiple structures, anharmonic effects, and various reaction pathways, each of which accounts for multidimensional tunneling. For the major channel (H abstraction from C2), the branching ratio (Γ) for both reactions decreases with increasing temperature (from 98% to 78% in the case of 2CB and 92% to 88% in the case of 2AB). The branching ratio of the C2–H abstraction is ∼90% and ∼91% at 298 K for the reaction of 2CB and 2AB, respectively. Conversely, the branching ratios for H abstractions from other C atoms in the molecule increase with temperature over the range of 200 to 400 K, collectively accounting for the remaining ∼10% for 2CB and ∼9% for 2AB at 298 K. The rate coefficients for the major channel decrease with temperature, leading to a negative temperature dependence in both cases. For 2CB and 2AB, the second major contributing channel is H abstraction from the C3 position. Combined, the contributions from H abstraction at the C3 and N atoms in 2AB are equivalent to that from H abstraction at the C3 atom in 2CB. The high branching observed at the C2 atom is attributed to the presence of an electronegative atom in both molecules. Additionally, the C2 atom, being secondary, contributes more significantly than the C3 atom. Other H atoms are primary, thus contributing less (<1%) to the overall kinetics. Similarly, the C2–H abstraction was reported to be the highest among all pathways in the case of 2-butanol.[68] When 2-butanol reacts with OH radicals, the branching ratios for H abstractions are as follows: C2 (51%) > C3 (45%) > C4 (1.5%) > C1 (1.2%) > O (1.1%).

Product analysis. The gas mixtures, consisting of 2CB or 2AB, H_2O_2, O_2, and N_2, were subjected to photolysis. To identify the products generated in the reactions, the gaseous mixture was fed into the GC-MS for analysis following photolysis. In the reaction of 2CB with OH radicals, the products formed are 2-butanone and 3-chloro-2-butanone. For the reactions of 2AB with OH radicals, the products are 2-butanone and 2-nitrobutane. The chromatograms of the products are depicted in Fig. 6 and the mass spectra for the products are shown in Fig. S5. Based on the products, the mechanisms for both reactions were proposed, as shown in Fig. 7. The following is the reaction mechanism for the reactions: the compound reacts with OH radicals, leading to the formation of the corresponding radical

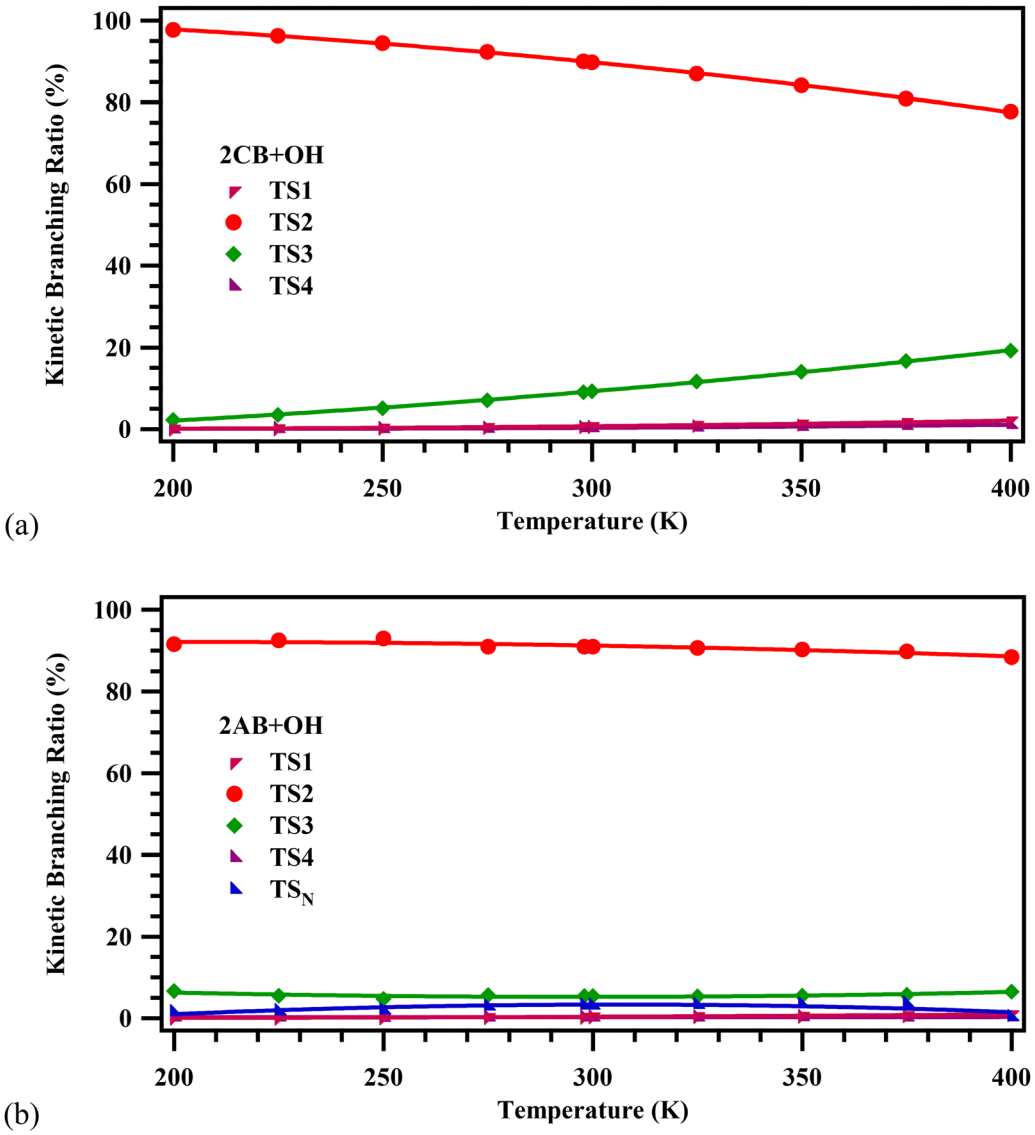

Fig. 5 Kinetic branching ratios (%) in the reactions of OH radicals with (a) 2CB and (b) 2AB.

intermediates. These radicals subsequently interact with molecular O_2 to generate peroxy radicals. The peroxy radicals undergo decomposition or rearrangement to form the corresponding alkoxy radicals. In both cases, the products formed through the main contributory reaction pathways were detected. The abstraction of a hydrogen atom from the C2 position leads to the formation of 2-butanone in both reactions. In the case of 2CB, 3-chloro-2-butanone is formed as a result of H abstraction from the C3 atom. However, the H abstraction from the C3 atom was not observed in the GC-MS study of 2AB. Instead, a significant alternate pathway involves the abstraction of an H atom from the N atom of 2AB by OH radicals, resulting in the formation of 2-nitrobutane, which was detected in the GC-MS. This observation highlights the differing reactivity of 2AB compared to 2CB and indicates the presence of an additional reaction pathway involving the nitrogen atom. The products formed in the reaction of 2CB with OH are analogous to those observed in the reaction of 2CB with Cl atoms. Specifically, both reactions form 2-butanone as a major product. This similarity suggests that the mechanisms of OH radical and Cl atom-mediated transformations of 2CB involve similar pathways.[33]

Atmospheric implications. The chemistry of the title compounds has atmospheric implications that can manifest locally, regionally, or globally. Residency duration of a species or lifetime (τ) determines whether it has short-term or long-term effects on the atmosphere. Reactivity with the main atmospheric oxidants is the principal factor that determines the residency period of a species in the atmosphere and its impact on air quality. The following defines the lifetimes that arise from a reaction with a particular oxidant (τ_{Ox}).

$$\tau_{Ox} = \frac{1}{\sum\{1/(k_{Ox}[Ox])\}}$$

Here, [Ox] indicates the average atmospheric concentration of oxidants, and k_{Ox} is the rate coefficient for the reaction between the chemical of interest and the oxidant Ox. The

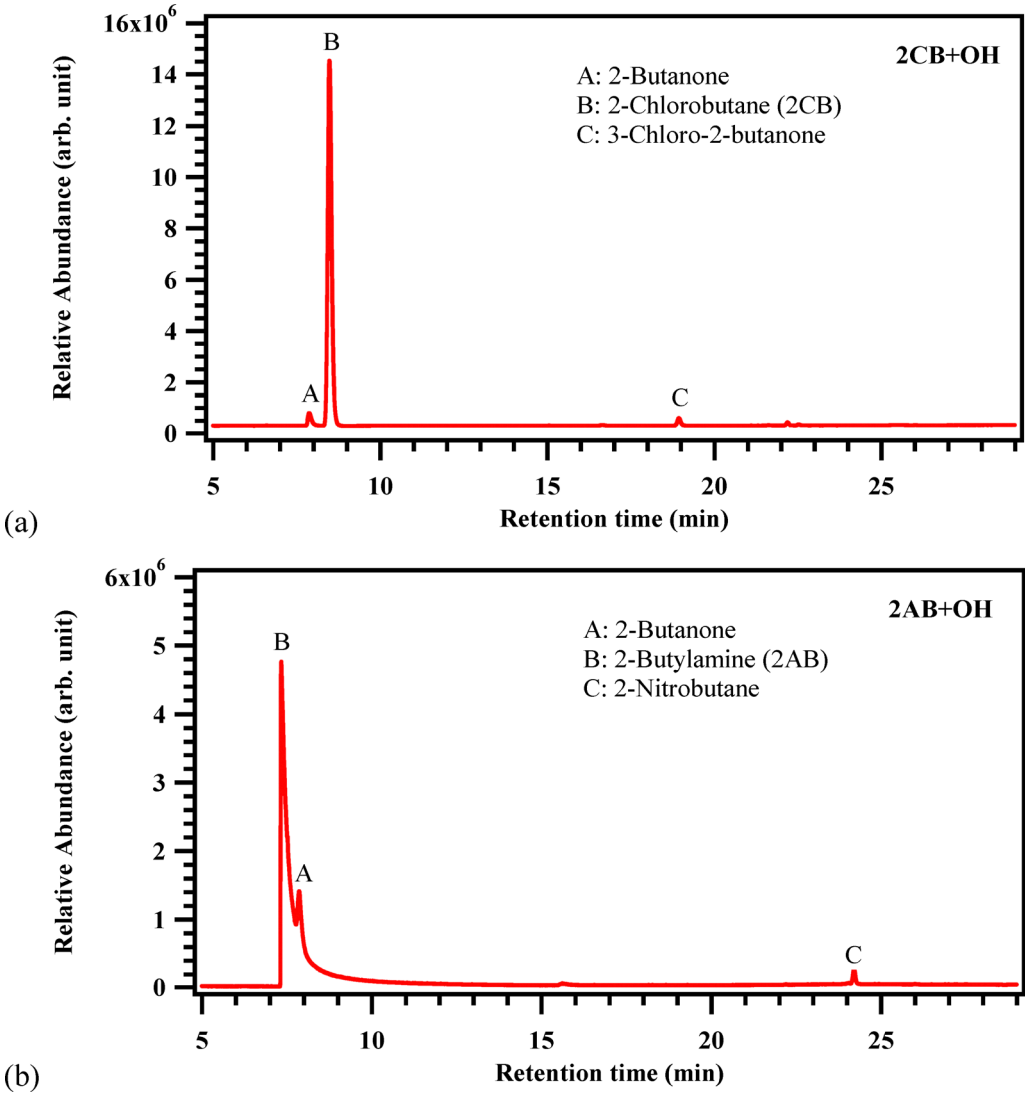

Fig. 6 Chromatograms for the reactions of (a) 2CB and (b) 2AB with OH radicals obtained using GC-MS.

atmospheric lifetimes of 2CB and 2AB have been estimated to be ~5 days and ~10 hours, respectively, at 298 K. While the lifetime of 2AB was determined by taking into account its reaction with OH radicals, the lifetime of 2CB was determined by taking into account both its reaction with OH radicals and Cl atoms. The experimental rate coefficients measured for OH-initiated reactions of 2CB and 2AB in the present study have been taken for the lifetime estimation, whereas the Cl-initiated reaction of 2CB was taken from the reported data by Kar and Rajakumar,[33] *i.e.*, 5.84×10^{-11} cm^3 molecule^{-1} s^{-1}. According to Prinn *et al.*,[78] the concentration of OH radicals was 9.7×10^5 radical cm^{-3}. The marine boundary layer (MBL) has a higher concentration of Cl atoms than the ambient condition. According to the most recent study by Wang *et al.*,[79] the Cl atom concentration was calculated to be 1200 atom cm^{-3} in MBL and 650 atom cm^{-3} under ambient conditions. In this context, other forms of their losses, like heterogeneous reactions, photolysis, and physical wet and dry deposition, are not considered. However, for most haloalkanes, they are anticipated to have minimal impact. Dry deposition of particles in the atmosphere is a significant pathway for eliminating pollutants from the air and depositing them onto the Earth's surface.[80] The impact of wet deposition is high for amine particulates due to their high water-solubility and acid-neutralizing capacity,[23] but dry deposition cannot be ignored in the dry season.[81] Thus, the lifetime of 2AB will be affected by the heterogenous loss in the atmosphere.

One of the key indicators of global climate change is radiative forcing (RF). Because of their C–Cl and C–N bonds, 2CB and 2AB can absorb radiation in the 500–895 cm^{-1} and 1000–1250 cm^{-1} ranges, respectively, which could make them strong greenhouse gases. To evaluate the effect of the molecules examined in this work on global warming, the RF can be calculated using Pinnock's equation.[82] It is detailed in the SI. For 2CB and 2AB, the RF was determined to be 0.025 and 0.085 W m^{-2} ppbv^{-1}, respectively. According to Hodnebrog *et al.*,[83] the lifetime corrected RFs for 2CB and 2AB were found to be 1.3×10^{-3} and 4.3×10^{-4} W m^{-2} ppbv^{-1}, respectively.

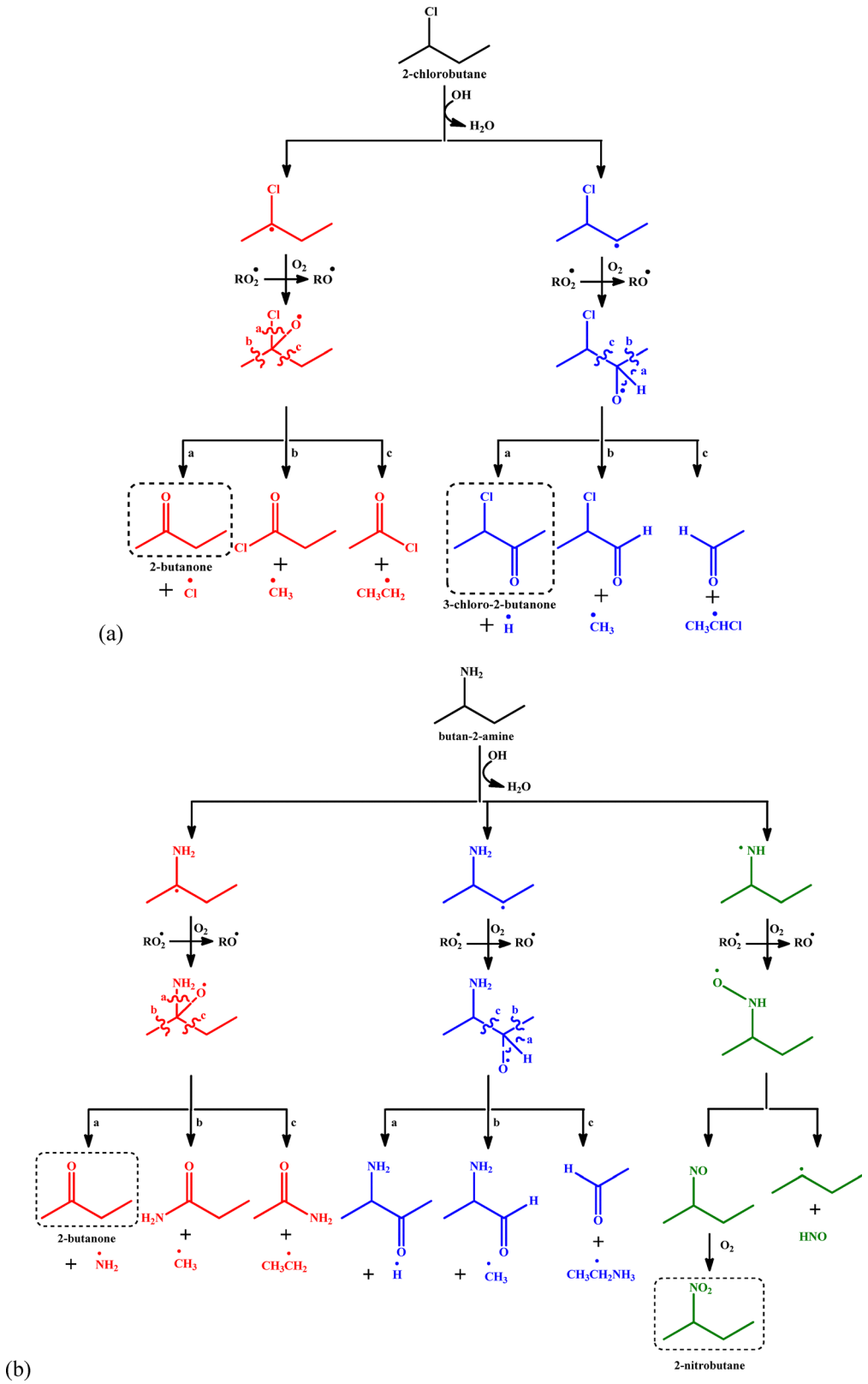

Fig. 7 The proposed mechanism for the formation of products in the reactions of (a) 2CB and (b) 2AB with OH radicals in the presence of O_2.

The global warming potential for the compounds 2CB and 2AB were estimated to be 0.0097 and 0.00035 for 100 years of time horizon. The lifetime of 2CB is longer than that of 2AB, leading to more lifetime-corrected RF than 2AB. A significant contribution of a compound to global warming results from its high concentration, prolonged lifespan, and impact on RF. In

addition, amines can form secondary aerosols, which can contribute to global warming and air quality.

The presence of N, S, Cl, and F atoms in the VOCs contributes to the acidification in the atmosphere. There has been a significant increase, ranging from three to over ten times, in the deposition of nitrogen from the atmosphere compared to levels before industrialization.[84] Both compounds studied in the current work could contribute to atmospheric acidification. The acidification potential was estimated for 2AB and 2CB to be 0.44 and 0.35, respectively. It is unity for SO_2, the most important gas leading to acidification, whereas the nitrogen oxides contribute the highest due to their larger emission compared to S compounds. It indicates that the studied compounds may have some influence on atmospheric acidification. It is observed that the N-containing compounds (2AB) have a slightly higher effect than that of the corresponding Cl-containing compound (2CB).

The OH-initiated reaction of 2CB yields carbonyl compounds or halogenated carbonyl compounds. These products are significant due to their potential in photochemical smog formation, which can exacerbate urban air pollution. Furthermore, halogenated carbonyl compounds are known to be carcinogenic, posing considerable risks to human health. In contrast, the OH-initiated reaction of 2AB typically generates carbonyl compounds or nitrogenated species. These nitrogenated compounds are particularly important in the atmosphere as they can contribute to forming atmospheric aerosols, which play a crucial role in climate dynamics and air quality.

Conclusions

Both experimental and computational methods were used to examine the kinetics of the reactions of 2CB and 2AB with OH radicals and showed a negative temperature dependence across the temperature range studied. The rate coefficient for the reaction of 2AB with OH radicals is higher than that of 2CB. In both reactions, the H abstraction from the αC (C2) atom is the major reaction pathway. A common product, 2-butanone, was detected in both reactions in the presence of O_2 using a GC-MS. The shorter lifetime of both compounds indicates their decomposition in the atmosphere near the source. Thus, 2CB may have a greater contribution to global warming relative to 2AB because of its longer lifetime. These two compounds may have a modest impact on atmospheric acidification, and 2AB exhibits a greater potential for acidification than 2CB. This kinetic data can be incorporated into the chemical modules of atmospheric models, informing policymakers as they shape strategies to enhance air quality.

Conflicts of interest

There is no conflicts of interest.

Data availability

The data supporting this article are provided in the SI. Supplementary information: PLP–LIF experimental data (Tables S1–S4); vibrational frequencies of stationary points (Tables S5 and S7); Cartesian coordinates of optimised geometries of stationary points (Tables S6 and S8); thermochemical parameters (Tables S9 and S10); barrier heights at the double-zeta level and CBS limit (Tables S11 and S12); T_1 diagnostic values (Table S13); computational rate coefficients (Tables S14 and S15); MS-T correction factors (Tables S16 and S17); kinetic branching ratio (Tables S18 and S19); optimised geometries of stationary points (Fig. S1 and S2); IRC plots (Fig. S3 and S4); mass spectra of products (Fig. S5); atmospheric implications; and calibration curves of MFCs. See DOI: https://doi.org/10.1039/d5cp00961h

Acknowledgements

Bishnupriya Kar expresses her gratitude to the Indian Institute of Technology Madras (IITM) for providing the fellowship. Balla Rajakumar thanks the BRNS, Government of India, for their financial support. The authors also wish to acknowledge the AQUA supercluster at IIT Madras for its support in computational calculations. They also acknowledge the Central Electronic Center at IIT Madras for helping them with technological problems.

References

1 D. W. Green, J. M. Lee, E. J. Kim, D. J. Lee and H. S. Jung, *Adv. Mater. Interfaces*, 2016, **3**(6), 1500411.
2 Q. Yin, Y. Shi, J. Wang and X. Zhang, *Chem. Soc. Rev.*, 2020, **49**(17), 6141–6153.
3 B. Gál, C. Bucher and N. Z. Burns, *Mar. Drugs*, 2016, **14**(11), 206.
4 Chemical Entities of Biological Interest (ChEBI). *sec*-Butylamine (CHEBI: 74526).
5 M. Tzatzarakis, A. M. Tsatsakis, A. Liakou and D. J. Vakalounakis, *J. Environ. Sci. Health, Part B*, 2000, **35**(4), 527–537.
6 A. Pendem, V. M. Pawar and S. Jayaraman, *J. Agric. Food Chem.*, 2010, **58**(16), 8904–8910.
7 N. Kaushal, N. Sharma and P. Sharma, *Curr. Microbiol.*, 2023, **80**(12), 381.
8 E. W. Day Jr, F. J. Holzer, J. B. Tepe, J. W. Eckert and M. J. Kolbezen, *Anal. Chem. J.*, 1968, **51**(1), 39–44.
9 J. A. Munoz-Delgado, *Int. J. Refrig.*, 1987, **10**(4), 229–233.
10 M. P. Clark, S. K. Laughlin, M. J. Laufersweiler, R. G. Bookland, T. A. Brugel, A. Golebiowski, M. P. Sabat, J. A. Townes, J. C. VanRens, J. F. Djung and M. G. Natchus, *J. Med. Chem.*, 2004, **47**(11), 2724–2727.
11 N. E. Benamara, M. Merabet-Khelassi, S. G. Lakoud, L. Aribi-Zouioueche and O. Riant, *ChemistrySelect*, 2021, **6**(48), 13941–13946.
12 B. Thitakamol, A. Veawab and A. Aroonwilas, *Int. J. Greenhouse Gas Control*, 2007, **1**(3), 318–342.
13 I. Schmeltz and D. Hoffmann, Nitrogen-containing compounds in tobacco and tobacco smoke, *Chem. Rev.*, 1977, **77**(3), 295–311.

14 A. Y. Ş. E. Yumak, K. Boubaker, P. Petkova and U. Ğ. U. R. Yahsi, *J. Mol. Struct.*, 2015, **1098**, 255–260.
15 J. Zielonka, R. Podsiadły, M. Czerwińska, A. Sikora, J. Sokołowska and A. Marcinek, *J. Photochem. Photobiol., A*, 2004, **163**(3), 373–379.
16 M. Villacampa, E. Diaz de Apodaca, J. R. Quintana and I. Katime, *Macromolecules*, 1995, **28**(12), 4144–4149.
17 M. M. Green, C. Khatri and N. C. Peterson, *J. Am. Chem. Soc.*, 1993, **115**(11), 4941–4942.
18 ChemicalBook—Chemical Products Search/2-chlorobutane CAS#: 78-86-4.
19 C. Su, R. Hopson and P. G. Williard, *Eur. J. Inorg. Chem.*, 2023, 4136–4141.
20 J. W. Eckert and M. L. Rahm, *Pestic. Sci.*, 1983, **14**(3), 220–228.
21 K. Hunter and D. Lindsay, *Pestic. Sci.*, 1981, **12**(3), 319–324.
22 S. E. Cornell, T. D. Jickells, J. N. Cape, A. P. Rowland and R. A. Duce, *Atmos. Environ.*, 2003, **37**(16), 2173–2191.
23 X. Ge, A. S. Wexler and S. L. Clegg, *Atmos. Environ.*, 2011, **45**(3), 524–546.
24 T. E. Graedel, D. T. Hawkins and L. D. Claxton, *Atmospheric chemical compounds: sources, occurrence and bioassay*, Elsevier, 2012.
25 N. E. Rabaud, S. E. Ebeler, L. L. Ashbaugh and R. G. Flocchini, *Atmos. Environ.*, 2003, **37**(7), 933–940.
26 S. M. Murphy, A. Sorooshian, J. H. Kroll, N. L. Ng, P. Chhabra, C. Tong, J. D. Surratt, E. Knipping, R. C. Flagan and J. H. Seinfeld, *Atmos. Chem. Phys.*, 2007, **7**(9), 2313–2337.
27 S. K. Brown, M. R. Sim, M. J. Abramson and C. N. Gray, *Indoor Air*, 1994, **4**(2), 123–134.
28 S. J. O'Doherty and L. J. Carpenter, Halogenated volatile organic compounds, *Volatile Org. Compd. Atmos.*, 2007, 173–220.
29 M. D. Hurley, T. J. Wallington, L. Laursen, M. S. Javadi, O. J. Nielsen, T. Yamanaka and M. Kawasaki, *J. Phys. Chem. A*, 2009, **113**(25), 7011–7020.
30 B. Kar and B. Rajakumar, *Atmos. Environ.*, 2024, **336**, 120717.
31 G. S. Madhu and B. Rajakumar, *Chemosphere*, 2024, **362**, 142566.
32 O. J. Nielsen, M. J. Javadi, M. S. Andersen, M. D. Hurley, T. J. Wallington and R. Singh, *Chem. Phys. Lett.*, 2007, **439**(1–3), 18–22.
33 B. Kar and B. Rajakumar, *Chemosphere*, 2023, **339**, 139664.
34 J. C. Loison, L. Ley and R. Lesclaux, *Chem. Phys. Lett.*, 1998, **296**(3–4), 350–356.
35 F. Joy and B. Rajakumar, *J. Phys. Chem. A*, 2025, **129**(27), 6057–6070.
36 F. Joy and B. Rajakumar, *Phys. Chem. Chem. Phys.*, 2023, **25**(11), 7901–7916.
37 A. Kumar, K. Mondal and B. Rajakumar, *J. Phys. Chem. A*, 2021, **125**(40), 8869–8881.
38 H. Keller-Rudek, G. K. Moortgat, R. Sander and R. Sörensen, *Earth Syst. Sci. Data*, 2023, **5**, 365–373.
39 Y. Zhao and D. G. Truhlar, *Acc. Chem. Res.*, 2008, **41**(2), 157–167.
40 Y. Zhao and D. G. Truhlar, *Theor. Chem. Acc.*, 2008, **120**, 215–241.
41 B. R. Giri, T. V. T. Mai, K. P. Shrestha, S. Giri, R. T. Naik, R. Verma, F. Mauss and L. K. Huynh, *Int. J. Chem. Kinet.*, 2025, **57**(6), 353–363.
42 M. E. Frisch, G. W. Trucks, H. B. Schlegel, G. E. Scuseria, M. Robb, J. R. Cheeseman, G. Scalmani, V. P. G. A. Barone, G. A. Petersson, H. J. R. A. Nakatsuji and X. Li, *Gaussian 16*, 2016.
43 R. Dennington, T. Keith and J. Millam, *GaussView, version 5*, 2009.
44 B. Kar and B. Rajakumar, *J. Phys. Chem. A*, 2025, **129**(23), 5137–5148.
45 B. R. Giri, T. V.-T. Mai, M. Assali, T. T. D. Nguyen, H. T. Nguyen, M. Szőri, L. K. Huynh, C. Fittschen and A. Farooq, *Phys. Chem. Chem. Phys.*, 2022, **24**(13), 7836–7847.
46 B. R. Giri, T. V. T. Mai, T. T. D. Nguyen, M. Szőri, L. K. Huynh and A. Farooq, *Combust. Flame*, 2022, **241**, 11215.
47 T. V. T. Mai, T. T. D. Nguyen, H. T. Nguyen, T. T. Nguyen and L. K. Huynh, *Environ. Sci. Technol.*, 2021, **55**(12), 7858–7868.
48 B. O. Milhøj and S. P. Sauer, *J. Phys. Chem. A*, 2015, **119**, 6516–6527.
49 J. Zheng, J. L. Bao, R. Meana-Pañeda, S. Zhang, B. J. Lynch, J. C. Corchado, Y.-Y. Chuang, P. L. Fast, W.-P. Hu, Y.-P. Liu, G. C. Lynch, K. A. Nguyen, C. F. Jackels, A. Fernandez Ramos, B. A. Ellingson, V. S. Melissas, J. Villà, I. Rossi, E. L. Coitiño, J. Pu, T. V. Albu, A. Ratkiewicz, R. Steckler, B. C. Garrett, A. D. Isaacson and D. G. Truhlar, *Polyrate-version 2017-C*, University of Minnesota, Minneapolis, MN, 2017.
50 J. Zheng, S. Zhang, J. C. Corchado, Y.-Y. Chuang, E. L. Coitiño, B. A. Ellingson and D. G. Truhlar, *Gaussrate 17*, University of Minnesota, Minneapolis, 2017.
51 J. C. Rienstra-Kiracofe, W. D. Allen and H. F. Schaefer, *J. Phys. Chem. A*, 2000, **104**, 9823–9840.
52 B. R. Giri, A. Farooq, M. Szőri and J. M. Roscoe, *Phys. Chem. Chem. Phys.*, 2022, **24**(8), 4843–4858.
53 R. A. Jara-Toro, J. A. Barrera, J. P. Aranguren-Abrate, R. A. Taccone and G. A. Pino, *J. Phys. Chem. A*, 2019, **124**, 229–239.
54 W. Tian, W. Wang, Y. Zhang and W. Wang, *Int. J. Quantum Chem.*, 2009, **109**(7), 1566–1575.
55 N. V. R. Nulakani and M. A. Ali, *Front. Chem.*, 2024, **12**, 1407355.
56 Á. Illés, Z. B. Rózsa, R. Thangaraj, E. D. Gombos, S. Dóbé, B. R. Giri and M. Szőri, *Chem. Phys. Lett.*, 2021, **776**, 138698.
57 J. Zheng, R. Meana-Pañeda and D. G. Truhlar, *Comput. Phys. Commun.*, 2013, **184**, 2032–2033.
58 J. Zheng and D. G. Truhlar, *J. Chem. Theory Comput.*, 2013, **9**, 1356–1367.
59 J. Zheng, S. L. Mielke, K. L. Clarkson and D. G. Truhlar, *Comput. Phys. Commun.*, 2012, **183**, 1803–1812.
60 M. W. Chase, NIST-JANAF thermochemical tables, *J. Phys. Chem. Ref. Data*, 1998, **28**, 1951.
61 R. Atkinson, *Int. J. Chem. Kinet.*, 1987, **19**, 799–828.
62 E. S. Kwok and R. Atkinson, *Atmos. Environ.*, 1995, **29**, 1685–1695.

63 M. E. Jenkin, R. Valorso, B. Aumont, A. R. Rickard and T. J. Wallington, *Atmos. Chem. Phys.*, 2018, **18**, 9297–9328.
64 C. J. Nielsen, H. Herrmann and C. Weller, *Chem. Soc. Rev.*, 2012, **41**, 6684–6704.
65 R. A. Perry, R. Atkinson and J. N. Pitts, *J. Chem. Phys.*, 1976, **64**, 5314–5316.
66 W. Tan, L. Zhu, T. Mikoviny, C. J. Nielsen, A. Wisthaler, P. Eichler, M. Müller, B. d'Anna, N. J. Farren and J. F. Hamilton, *J. Phys. Chem. A*, 2018, **122**, 4470–4480.
67 E. Jiménez, B. Lanza, A. Garzón, B. Ballesteros and J. Albaladejo, *J. Phys. Chem. A*, 2005, **109**, 10903–10909.
68 J. Zheng, G. A. Oyedepo and D. G. Truhlar, *J. Phys. Chem. A*, 2015, **119**, 12182–12192.
69 M. R. McGillen, M. Baasandorj and J. B. Burkholder, *J. Phys. Chem. A*, 2013, **117**, 4636–4656.
70 R. Atkinson, D. L. Baulch, R. A. Cox, J. N. Crowley, R. F. Hampson Jr, J. A. Kerr, M. J. Rossi and J. Troe, Summary of evaluated kinetic and photochemical data for atmospheric chemistry, IUPAC Subcommittee on gas kinetic data evaluation for atmospheric chemistry, 2001.
71 S. C. Herndon, T. Gierczak, R. K. Talukdar and A. R. Ravishankara, *Phys. Chem. Chem. Phys.*, 2001, **3**, 4529–4535.
72 F. Markert and O. J. Nielsen, *Chem. Phys. Lett.*, 1992, **194**, 123–127.
73 J. H. Kasner, P. H. Taylor and B. Dellinger, *J. Phys. Chem.*, 1990, **94**, 3250–3253.
74 M. Yujing and A. Mellouki, *Phys. Chem. Chem. Phys.*, 2001, **3**, 2614–2617.
75 L. Onel, L. Thonger, M. A. Blitz, P. W. Seakins, A. J. C. Bunkan, M. Solimannejad and C. J. Nielsen, *J. Phys. Chem. A*, 2013, **117**, 10736–10745.
76 R. Atkinson, R. A. Perry and J. N. Pitts, *J. Chem. Phys.*, 1977, **66**, 1578–1581.
77 R. Atkinson, R. A. Perry and J. N. Pitts, *J. Chem. Phys.*, 1978, **68**, 1850–1853.
78 R. G. Prinn, J. Huang, R. F. Weiss, D. M. Cunnold, P. J. Fraser, P. G. Simmonds, A. McCulloch, C. Harth, P. Salameh, S. O'Doherty, R. H. J. Wang, L. Porter and B. R. Miller, *Science*, 2001, **292**, 1882–1888.
79 X. Wang, D. J. Jacob, S. D. Eastham, M. P. Sulprizio, L. Zhu, Q. Chen, B. Alexander, T. Sherwen, M. J. Evans, B. H. Lee, J. D. Haskins, F. D. Lopez-Hilfiker, J. A. Thornton, G. L. Huey and H. Liao, *Atmos. Chem. Phys.*, 2019, **19**, 3981–4003.
80 K. Zhang, B. Z. Zhang, S. M. Li, L. M. Zhang, R. Staebler and E. Y. Zeng, *Atmos. Environ.*, 2012, **57**, 41–48.
81 F. Liu, X. Bi, G. Zhang, L. Peng, X. Lian, H. Lu, Y. Fu, X. Wang, P. Peng and G. Sheng, *Atmos. Environ.*, 2017, **171**, 279–288.
82 S. Pinnock, M. D. Hurley, K. P. Shine, T. J. Wallington and T. J. Smyth, *J. Geophys. Res.: Atmos.*, 1995, **100**, 23227–23238.
83 Ø. Hodnebrog, M. Etminan, J. S. Fuglestvedt, G. Marston, G. Myhre, C. J. Nielsen, K. P. Shine and T. J. Wallington, *Rev. Geophys.*, 2013, **51**, 300–378.
84 J. N. Galloway, W. H. Schlesinger, H. Levy, A. Michaels and J. L. Schnoor, *Global Biogeochem. Cycles*, 1995, **9**, 235–252.